Catalysis Science & Technology

# Synthesis and Molecular Structure of Model Silica-supported Tungsten oxide Catalysts for Oxidative Coupling of Methane (OCM)

| | |
|---|---|
| Journal: | *Catalysis Science & Technology* |
| Manuscript ID | CY-ART-02-2020-000289.R1 |
| Article Type: | Paper |
| Date Submitted by the Author: | 14-Mar-2020 |
| Complete List of Authors: | Kiani, Daniyal; Lehigh University, Chemical and Biomolecular Engineering<br>Sourav, Sagar; Lehigh University, Chemical and Biomolecular Engineering<br>Wachs, Israel; Lehigh University, Chemical Engineering<br>Baltrusaitis, Jonas; Lehigh University, Chemical and Biomolecular Engineering; |
| | |

# Synthesis and Molecular Structure of Model Silica-supported Tungsten oxide Catalysts for Oxidative Coupling of Methane (OCM)

Daniyal Kiani†, Sagar Sourav†, Israel E. Wachs* and Jonas Baltrusaitis*

Department of Chemical and Biomolecular Engineering, Lehigh University, B336 Iacocca Hall, 111 Research Drive, Bethlehem, PA 18015, USA

†DK and SS contributed equally

*Corresponding authors: iew0@lehigh.edu, job314@lehigh.edu

**Abstract.** The molecular and electronic structures, and chemical properties of the active sites on the surface of supported $Na_2WO_4/SiO_2$ catalysts used for Oxidative Coupling of Methane (OCM) are poorly understood. Model $SiO_2$-supported, Na-promoted tungsten oxide catalysts ($Na-WO_x/SiO_2$) were systematically prepared using various Na- and W-precursors using carefully controlled Na/W molar ratios and examined with *in situ* Raman, UV-Vis DR, $CO_2$-TPD-DRIFT and $NH_3$-TPD-DRIFT spectroscopy. The traditionally prepared catalyst corresponding to 5% $Na_2WO_4$ nominal loading, Na/W molar ratio of 2, were synthesized from the aqueous $Na_2WO_4{\cdot}2H_2O$ precursor. After calcination at 800°C, the initially amorphous $SiO_2$ support crystallized to the cristobalite phase and the supported sodium tungstate phase consisted of both crystalline $Na_2WO_4$ nanoparticles (Na/W=2) and a dispersed surface $Na-WO_4$ sites (Na/W<2). Catalysts prepared via a modified impregnation method using individual precursors of NaOH + AMT, such that the Na/W molar ratio remained well below 2, the resulting $SiO_2$ remained amorphous and the supported sodium-tungstate phase only consisted of dispersed surface $Na-WO_4$ sites (Na/W<2). The dispersed surface $Na-WO_4$ sites were isolated, more geometrically distorted, less basic in nature, and more reducible than the crystalline $Na_2WO_4$ nanaoparticles. The $CH_4+O_2$-TPSR results reveal that the isolated, dispersed surface $Na-WO_4$ sites are significantly more selective towards $C_2$ products, and initiate $C_2H_6$ formation at higher temperature than the traditionally-prepared catalysts that contains both crystalline $Na_2WO_4$ nanoparticles and dispersed surface $Na-WO_4$ sites. These findings demonstrate that the isolated, dispersed phase $Na-WO_4$ sites on the $SiO_2$ support surface are the catalytic selective-active sites for OCM reaction.

Keywords: OCM, $Na_2WO_4$, In Situ, Raman, DRIFTS, UV-VisDR, TPR, TPSR, active sites

## 1. Introduction:

Catalytic oxidative coupling of methane (OCM) is a single-step process for the conversion of methane ($CH_4$) into value-added products such as ethylene ($C_2H_4$).[1] Since the pioneering work of Kellar and Bhasin in 1982[2], hundreds of catalysts comprised of oxides of alkali, alkaline-earth, and transition metals have been tested for OCM. With the new developments in *in situ* and *operando* measurements, interest in understanding and designing an efficient OCM catalyst has experienced a renewal in the past decade.[3–6] Most of the catalysts reported for OCM were deemed unsuitable for large-scale commercialization due to the lack of long-term stability at high operational temperatures above 800°C, and over-oxidation of hydrocarbons to $CO_x$.[7,8] In this regard, the $SiO_2$-supported $MnO_x$-$Na_2WO_4$/$SiO_2$ mixed metal oxide catalyst is one of the few catalysts that exhibit high thermal stability and promising $C_2$ product yield (~28%).[7,8]

First reports on the $SiO_2$-supported $MnO_x$-$Na_2WO_4$/$SiO_2$ catalyst for OCM appeared in the early-90s[9–12]. Since then, research efforts have largely remained focused on increasing the $C_2$ yield by adding promoters, changing support materials, trying various synthesis routes, etc[7,8] To date, almost all studies conducting characterization of this catalyst found crystalline phases including $Na_2WO_4$, $Mn_2O_3$ and α-cristobalite phase of the $SiO_2$ support along with $Na_2W_2O_7$, $MnWO_4$ and $MnMn_6SiO_2$, depending on the catalyst preparation method and precursors used.[8] Surprisingly, in the absence of convincing supporting *surface* site analysis evidence, these crystalline phases have been proposed as active phases towards the catalytic OCM reaction.[7,8,13,14] On the contrary, an *in situ* XRD study recently showed that crystalline $Na_2WO_4$ was not present under OCM reaction conditions (>800°C) since the $Na_2WO_4$ crystal melts at ~698°C.[15,16] Additionally, the intensity of the XRD peaks for the crystalline $Mn_2O_3$ and α-cristobalite were found to significantly decrease during OCM, while the intensity of peaks from $Mn_3O_4$ and β-cristobalite phase increased due to phase transformations occurring at OCM relevant temperatures.[8,15,16] These *in situ* XRD results have highlighted that the crystalline phases of $Na_2WO_4$, $Mn_2O_3$ and α-cristobalite are not present under OCM reaction conditions and cannot be responsible for the OCM activity, in contrary to previous reports.[8] Unfortunately, information on the stable and active surface structures present on the $MnO_x$-$Na_2WO_4$/$SiO_2$ catalyst at elevated temperatures is largely missing from the literature. Further, prior investigations analyzed the catalysts only under ambient conditions - air-exposed, at room temperature.

Although XRD can readily detect crystalline phases with long-range order, it cannot detect phases lacking long-range order (e.g., amorphous 2D/3D phases and crystalline nanoparticles smaller than 3 nm). In contrast, Raman spectroscopy is better suited to systematically study and understand the molecular structure and identity of phases present on the catalyst support, because it can readily detect and discriminate between amorphous 2D and crystalline 3D phases as well as crystalline nanoparticles lacking long-range order (<3 nm).[17] The few earlier works that provide Raman spectroscopic characterization of supported $MnO_x$-$Na_2WO_4$/$SiO_2$ catalysts[10,11,18,19] collected information under ambient conditions where the catalyst surface is hydrated by ambient water molecules and differs significantly from the catalyst surface under reaction conditions at elevated temperatures. These reports also contain incorrect and/or unclear Raman band assignments. For example (a) a Raman band at ~950 $cm^{-1}$ was observed, but not assigned[11] and (b) the distorted tetrahedral $WO_4$ sites from crystalline $Na_2WO_4$ and $Na_2W_2O_7$ bulk phases were incorrectly assigned as $WO_4$ sites anchored to $SiO_2$ surface.[10,19] *Surface* molecular structures of metal oxides will structurally differ from *bulk* crystalline phases and will be the ones responsible for the structure/reactivity during OCM.[20–23] Recent studies using *in situ* Raman spectroscopy have elucidated the structure of different molecular geometries possible for a $SiO_2$-supported 2D-dispersed tungsten oxide ($WO_x$) phase under dehydrated conditions and elevated temperatures.[17,24–27] Specifically, the dispersed $WO_x$ sites on the $SiO_2$ support exhibit Raman bands at ~1015 and ~985 $cm^{-1}$ from mono-oxo $O{=}W(O\text{-}Si)_4$ and di-oxo $(O{=})_2W(O\text{-}Si)_2$ sites, respectively.[27] When the maximum dispersion limit of surface $WO_x$ sites on $SiO_2$ is exceeded, the excess tungsten oxide forms 3D crystalline NPs.[28] Likewise, in the presence of Na, as in the OCM catalyst under discussion, Na-coordinated $WO_x$ sites in the dispersed phase (never reported before) and crystalline $Na_2WO_4$ (Raman: 925-927, 810, 303$cm^{-1}$)[26,29] can co-exist. A schematical summary of the crystalline phases and molecular surface structures of the $SiO_2$-supported $WO_x$ systems are shown in **Figure 1**. Namely, (a) isolated surface di-oxo sites ($[O{=}]_2WO_2$) - $WO_4$, (b) oligomeric surface mono-oxo sites, $WO_x$ (x>=2) and (c) crystalline $WO_3$ nanoparticles (NPs) - $WO_6$.[27,17]

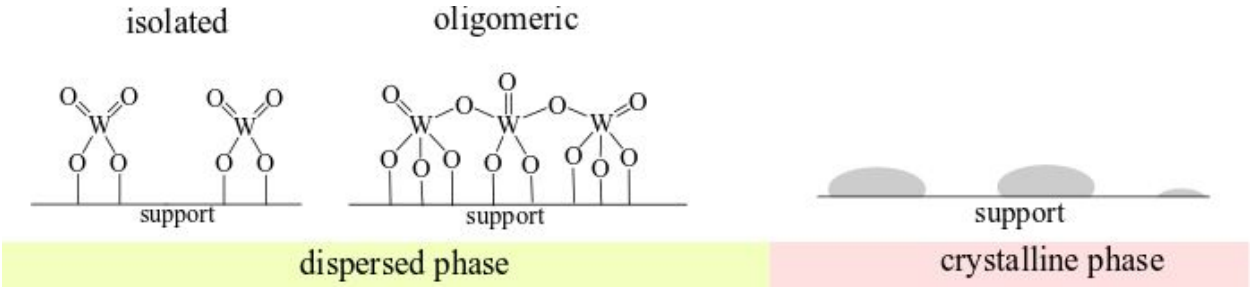


**Figure 1.** Schematic representation of possible structural and phase compositions of tungsten oxide-based catalysts on the $SiO_2$ support.

The ability to synthesize and spectroscopically characterize well-defined supported tungsten oxide catalytic sites is essential for establishing conclusive structure-function relationships for OCM.[27,17] This study aims to systematically study the structure of Na-$WO_x$ sites supported on $SiO_2$. Specifically, the goal is to identify phases, elucidate molecular level structural details, and shed light on fundamental properties of potentially OCM-relevant catalytic sites by tuning the synthesis protocol and adjusting the Na/W molar ratio in a bi-metal oxide configuration containing Na-$WO_x$ sites. Herein, we report on the molecular and electronic structures of the $WO_x$-based OCM catalytic sites, their domain sizes, their surface properties and their OCM performance. We highlight the effect of using different metal oxide precursors and tuning the Na/W molar ratio of active metal oxides on the final catalyst structure and properties. The catalysts were characterized using *in situ* Raman spectroscopy, *in situ* UV-Vis diffuse reflectance spectroscopy and probed using $H_2$-TPR (temperature-programmed reduction), $CH_4$+$O_2$-TPSR (temperature-programmed surface reaction), $NH_3$-TPD-, (temperature-programmed desorption) and $CO_2$-TPD-DRIFTS (diffuse reflectance infrared Fourier transformed spectroscopy).

## 2. Experimental

### a. Catalyst synthesis.

The $SiO_2$ support (Cabot CAB-O-SIL® EH5 with a surface area of ~332 $m^2/g$) was first treated with water, then allowed to dry overnight at room temperature before final calcination at 500°C for 4 hours under flowing air. This treatment increases the density and surface hydroxyls of the $SiO_2$ support. The dried $SiO_2$ obtained after calcination was then crushed into a fine powder. The resulting pore volume of the $SiO_2$ powder was determined to be ~0.8 ml/g and was utilized for all

catalyst preparation steps via incipient-wetness impregnation (IWI) of the metal oxide aqueous solutions unless mentioned otherwise.

To prepare the supported $Na_2WO_4/SiO_2$ catalyst with stoichiometric amounts of Na and W oxides, the conventional $Na_2WO_4 \cdot 2H_2O$ (Sigma-Aldrich, 99%) precursor was used. Given that the crystalline $Na_2WO_4$ phase is not stable under the high-temperature OCM reaction conditions,[15,16] the individual precursors for Na (NaOH (GR ACS, 97%); $Na_2CO_3$ (Aldrich, 99%) and $NaNO_3$ (Sigma-Aldrich, 99%)) and W (ammonium meta tungstate (AMT, Pfaltz & Bauer, 99.5%) were also utilized in the synthesis of the catalysts. For all preparations, the loadings of the Na and W precursors were maintained to correspond to ~5% $Na_2WO_4/SiO_2$ on a weight basis. After the incipient-wetness impregnation of the metal oxide aqueous solution precursors onto the $SiO_2$ support, the samples were allowed to initially dry overnight at room temperature and an additional drying for 2 hours at 120°C before final calcination at 800°C for 8 hours under flowing air.

Non-stoichiometric catalysts with the metal oxides fully dispersed on the $SiO_2$ support were also prepared using a modified IWI method.[30] A NaOH aqueous solution corresponding to the pore-volume equivalent of ~0.8 ml/g was impregnated onto the $SiO_2$ support and the sample was initially dried overnight, then at 120°C in an oven under flowing air for 2 hours, and finally calcined at 700°C under airflow for 2 hours. The resultant supported $Na/SiO_2$ sample, with pore volume equivalent of ~0.7 ml/g, was subsequently impregnated with the desired aqueous concentration of W in the form of AMT ($(NH_4)_xW_{12}O_{28}$; Alfa Aesar, #44792). The resultant solid was dried overnight, then at 120°C for 2 hours in airflow and finally calcined at 500°C for 4 hours under flowing air. The final catalysts were denoted as $aW/bNa/SiO_2$ where a=weight % metal loading of $WO_x$ and b= weight % metal loading of Na. A similar structure and properties were observed for a series of similar catalysts calcined at 800°C instead of 500°C. However, the sample prepared via 500°C calcination did not undergo severe sintering typical of higher temperature calcination, enabling easier characterization of the pre-reaction catalytic sites.

**b. *In situ* Raman spectroscopy.**

The *in situ* Raman spectra of the Na coordinated $WO_x/SiO_2$ supported catalysts were obtained with Horiba-Jobin Yvon LabRam HR instrument equipped with three laser excitations (532, 442, and 325 nm) and liquid $N_2$-cooled CCD detector (Horiba-Jobin Yvon CCD-3000 V). The 442 nm laser was chosen for spectral accumulation since it minimizes sample fluorescence from the $SiO_2$

supported catalysts. The wavenumber calibration was checked using a standard silicon wafer with a Raman vibration at 520.7 $cm^{-1}$. A confocal microscope with a 50x objective (Olympus BX-30-LWD) was utilized for focusing the laser on the catalysts. Typically, the spectra were collected for 60 s/scan for a total of three scans with a 1000 μm hole with a spectral resolution of ~1 $cm^{-1}$. Approximately 15-20 mg of each catalyst in powder form (100-150 μm size range) was loaded into an environmental cell (Harrick, HVC-DR2) with a quartz window with O-ring seals, which was kept cool by circulating cooling water. The *in situ* Raman spectra of the catalysts were collected at 400°C after dehydration in 10% $O_2$/Ar (~30 cc/min) for 60 min.

**c. *In situ* UV-Vis diffuse reflectance spectroscopy (DRS).**

The *in situ* UV−Vis spectra of the catalysts were obtained using a Varian Cary 5E UV−Vis−NIR spectrophotometer with a Harrick Praying Mantis accessory. Approximately 15−20 mg of each catalyst in powder form was loaded into an *in situ* Harrick HVCDR2 environmental cell. The UV-Vis spectra of the catalyst samples were collected at 400, 120, and 25°C in the 200−800 nm wavelength range after dehydration (10% $O_2$/Ar, ~30 cc/min) for 60 min at 400°C, using a scan rate of 15 nm/min and a signal averaging time of 0.6 s. MgO was used as a standard for obtaining the background absorbance and was subtracted from the sample absorbance. Kubelka−Munk function $F(R_\infty)$ was calculated from the background-subtracted absorbance data of the UV−Vis spectrum of each sample. The edge energy ($E_g$), or bandgap, was determined by finding the intercept of the straight line for the low-energy rise of a plot of $[F(R_\infty)hv]^2$ versus $hv$, where $hv$ is the incident photon energy. An example of this calculation can be found in literature.[31]

**d. Temperature programmed techniques.**

**$H_2$-TPR**. The $H_2$-TPR experiments were carried out using the AMI-200 (Altamira Instruments) with an integrated TCD detector to record the consumption of $H_2$ in the exiting gases. Approximately 30 mg of each catalyst sample was loaded (sandwiched between the quartz wool beds) into a U-tube sample holder. The catalyst samples were first dehydrated under 10% $O_2$/Ar (~30 cc/min) at 400°C for 60 min, then cooled down to 100°C. The $H_2$-TPR experiments were then performed by ramping the temperature under 10% $H_2$/Ar (30 cc/min) at a rate of 10°C/min from 100 to 1000°C.

**$CH_4$+$O_2$-TPSR.** The $CH_4$+$O_2$-TPSR experiments were also carried out in the AMI-200 system. For these experiments, the Dymaxion Dycor mass spectrometer (DME100MS) was utilized for residual gas analysis. Approximately 30 mg of each catalyst sample was loaded (sandwiched between quartz wool beds) into a quartz U-tube sample holder. The catalyst samples were first dehydrated under 10% $O_2$/Ar (~30 cc/min) at 400°C for 60 minutes, then ramped up to 900°C under an OCM gas mixture (~25 cc/min of $CH_4$ and ~40 cc/min of dry air) and held for 2 hours at 900°C in order to condition the catalyst under OCM reaction conditions. The catalyst was subsequently cooled to 100°C under the OCM gas mixture and then purged with Ar (~30 cc/min) for 30 minutes. At 100°C, a very dilute gas mixture of $CH_4$+$O_2$ ($CH_4$ of ~5 cc/min, 10% $O_2$/Ar of ~15 cc/min and Ar: ~80 cc/min) was introduced and the temperature was ramped up to 850°C at 10°C/min while analyzing the product gas stream with the online mass spectrometer. The dilution was necessary to prevent damaging the mass spectrometer filament under high $O_2$ concentrations in the OCM reaction mixture. For the detection of different gases, the following *m/z* values were used: $CH_4$ (*16*); $C_2H_4$ (*26*); CO (*28*), $C_2H_6$ (*30*); $O_2$ (*32*); Ar (*40*) and $CO_2$ (*44*). The fragmentation patterns were utilized to find out the Mass Spec signal contributions from individual gases for overlapping *m/z* values. All reactants' and products' signals were normalized with Ar signal, used as an internal standard. Further, the calibration curves were obtained for each reactant ($CH_4$ and $O_2$) and product ($C_2H_6$, $C_2H_4$, CO and $CO_2$) for quatification of mass spectrometer signals of these gases during the experiments. For calibration curve development, at least three different amount of each gas, diluted in Ar (to make a total flow of ~50 cc/min), were utilized to enhance accuracy. The conversion (% *X*) of $CH_4$ and $O_2$ were determined by the following formula:

$$\% X = \frac{n_0 - n}{n_0} \times 100$$

where, $n_0$ is the moles of $CH_4$ or $O_2$ in the reactant stream and $n$ is the moles of $CH_4$ or $O_2$ in the product stream.

The selectivity (% *S*) of each product was determined using the following formula:

$$\% S_i = \frac{n_{C_i}}{\sum n_{C_i}} \times 100$$

where, $n_{C_i}$ denotes the number of moles of C atoms present in product *i*.

Lastly, the yield (% $Y$) of any product $i$ was determined by:

$$\frac{\%\, X_{CH_4} \times \%\, S_i}{100}$$

**Surface properties: $NH_3$-, $CO_2$-TPD-DRIFTS.**

The *in situ* DRIFT spectra were collected with a Thermo Nicolet iS50 FT-IR spectrometer equipped with a Harrick Praying Mantis attachment (model DRA-2) for diffuse reflectance spectroscopy. Spectra were taken using an MCT detector with a resolution of ~4 $cm^{-1}$ and an accumulation of 96 scans. Approximately ~20 mg of each catalyst in powder form was loaded into an environmental cell (HVC-DR2, Harrick Scientific). The collection of the initial background was performed by first optimizing the beam path and IR absorption signal using the height of the full Harrick sample cup then removing the Harrick cell and placing a reflective mirror in the laser path. A spectrum was collected using the reflective mirror and was used as the background spectrum throughout the experiment. The catalysts were first cleaned and dehydrated at 400°C under 10%$O_2$/$N_2$ gas mixture at ~30 ml/min flow rate, cooled to 120°C under 10% $O_2$/$N_2$ and flushed with UHP5.0 $N_2$ (Praxair Prospec) at 30 ml/min flow rate for ~15 minutes. The catalysts were then subjected to gas adsorption at 120°C (1% $NH_3$ in $N_2$ or 10% $CO_2$ in $N_2$ or UHP5.0 $N_2$ at 30 ml/min flow rate through a methanol containing bubbler) for ~30 minutes followed by flushing with UHP5.0 $N_2$ at 30 ml/min flow rate for another 30 min to remove residual physisorbed molecules. The temperature was subsequently ramped from 120 to 400°C at 10°C/min, while a spectrum was collected every minute (96 accumulations) with a spectral resolution of ~4 $cm^{-1}$. The spectra of the dehydrated catalyst were subtracted from the spectra of the catalysts containing adsorbed gases at the same temperature.

## 3. Results

### a. *In situ* Raman spectroscopy of model supported Na-$WO_x$/$SiO_2$ catalysts

The *in situ* dehydrated Raman spectra of the model catalysts corresponding to 5%$Na_2WO_4$/$SiO_2$ nominal composition are presented in **Figure 2**. As shown in **Figure 2a**, for all catalysts with Na/W molar ratio of 2, which mimic the stoichiometry of the $Na_2WO_4$ crystals and irrespective of the precursor choice, the $SiO_2$ support is present in the β-cristobalite phase with corresponding bands labeled as '#'. In presence of Na, the starting amorphous $SiO_2$ converts to crystalline

cristobalite during the calcination step at ~800°C. The exclusive presence of the β-cristobalite phase of $SiO_2$ in the *in situ* Raman is due to the α-cristobalite transformation into β-cristobalite above 250°C, as shown in **Figure S1**. The Raman spectra of the supported 5% $Na_2WO_4/SiO_2$ catalysts prepared using $Na_2WO_4{\cdot}2H_2O$, NaOH+AMT and $Na_2CO_3$+AMT exhibit Raman bands at 925, 810 and 303 $cm^{-1}$ that are are characteristic of crystalline $Na_2WO_4$.[26] These catalysts also possess a small Raman band at 943 $cm^{-1}$, appearing as a shoulder to the 925 $cm^{-1}$ band, which does not belong to crystalline $Na_2WO_4$. The deconvolution of the bands present between 900-960 $cm^{-1}$ is shown in **Figure S2**. The Raman spectrum of the supported 5% $Na_2WO_4/SiO_2$ catalyst prepared using $NaNO_3$+AMT only exhibits a weak and broad Raman band at 932 $cm^{-1}$ and no sharp bands due to the crystalline $Na_2WO_4$. Such spectral features suggest the presence of a poorly-ordered phase composed of Na- and W-oxides. The origin of the broad Raman band in the 930-950 $cm^{-1}$ range shown in **Figure 2a** is not immediately clear. It can be hypothesized that this band originates due to the Na-coordinated $WO_x$ amorphous sites (Na-$WO_x$) present on the $SiO_2$ surface.

Model catalysts with Na/W molar ratio from 0.0 to 1.6 were synthesized and characterized as shown in **Figure 2b**. Besides the catalyst with Na/W molar ratio of 1.6, none of the catalysts exhibit the sharp Raman bands at 925, 810 and 303 $cm^{-1}$ corresponding to crystalline $Na_2WO_4$ indicating that only a dispersed Na-$WO_x$ phase is present on the $SiO_2$ support. Moreover, Raman bands corresponding to the crystalline cristobalite phase of $SiO_2$ support were not observed in these samples, indicating that the $SiO_2$ support is present in its amorphous phase. Specifically, the supported 5% $WO_x/SiO_2$ catalyst without any Na-dopant (Na/W=0) exhibits three characteristic Raman bands at 1015, 983 and 350 $cm^{-1}$ which correspond to the stretching and bending modes of the mono-oxo $WO_5$, $O{=}WO_4$, and the di-oxo $WO_4$ ($[O{=}]_2WO_2$) sites on the $SiO_2$ surface, respectively.[26,27] Addition of 0.2% Na to the supported 5%$WO_x/SiO_2$ catalyst to yield Na/W=0.3 results in a redshift of the W=O Raman vibration from 983 to 971 $cm^{-1}$. As the Na concentration is further increased to yield larger Na/W molar ratios 0.6 and 1, the W=O band vibration redshifts further to 964 and finally to 941 $cm^{-1}$, respectively. At the highest concentration of Na, with Na/W molar ratio 1.6, two Raman bands are present at 927 and 943 $cm^{-1}$. The band at 927 $cm^{-1}$ belongs to the crystalline $Na_2WO_4$ nanoparticles while the band at 943 $cm^{-1}$ belongs to surface $WO_x$ sites coordinated to Na (Na-$WO_x$) as revealed by the spectra of the catalysts with lower Na/W ratios.

Next, the influence of specific Na precursors on the non-stoichiometric catalysts with low Na content (8% $WO_x$ /0.4% $Na/SiO_2$; Na/W= ~0.4) are presented in **Figure 2c** and reveal the precursor-dependence. The catalyst prepared using AMT+NaOH precursor yielded only the fully dispersed phase with surface Na-$WO_x$ sites (~969 $cm^{-1}$) without any crystalline phases like $Na_2WO_4$ (~925, 810 and 303 $cm^{-1}$) or $WO_3$ (715 and 807 $cm^{-1}$).[26,27] However, when $NaNO_3$ is employed as the Na precursor, mixed phases were observed, with crystalline $WO_3$ exhibiting sharp, intense bands at 715 and 807 $cm^{-1}$,[26] and dispersed phase Na-$WO_x$ surface sites at 969 $cm^{-1}$. When $Na_2CO_3$ precursor was used, Raman bands are present from surface Na-$WO_x$ sites (~969 $cm^{-1}$) along with amorphous, poorly-ordered $WO_3$ NPs (~782 $cm^{-1}$).[32] The surface Na-$WO_x$ sites are dominant in all the supported 8% $WO_x$ /0.4% $Na/SiO_2$ catalysts since the Raman cross-sections of crystalline and poorly-ordered $WO_3$ NPs are orders of magnitude greater than the surface Na-$WO_x$ sites.[33,34]

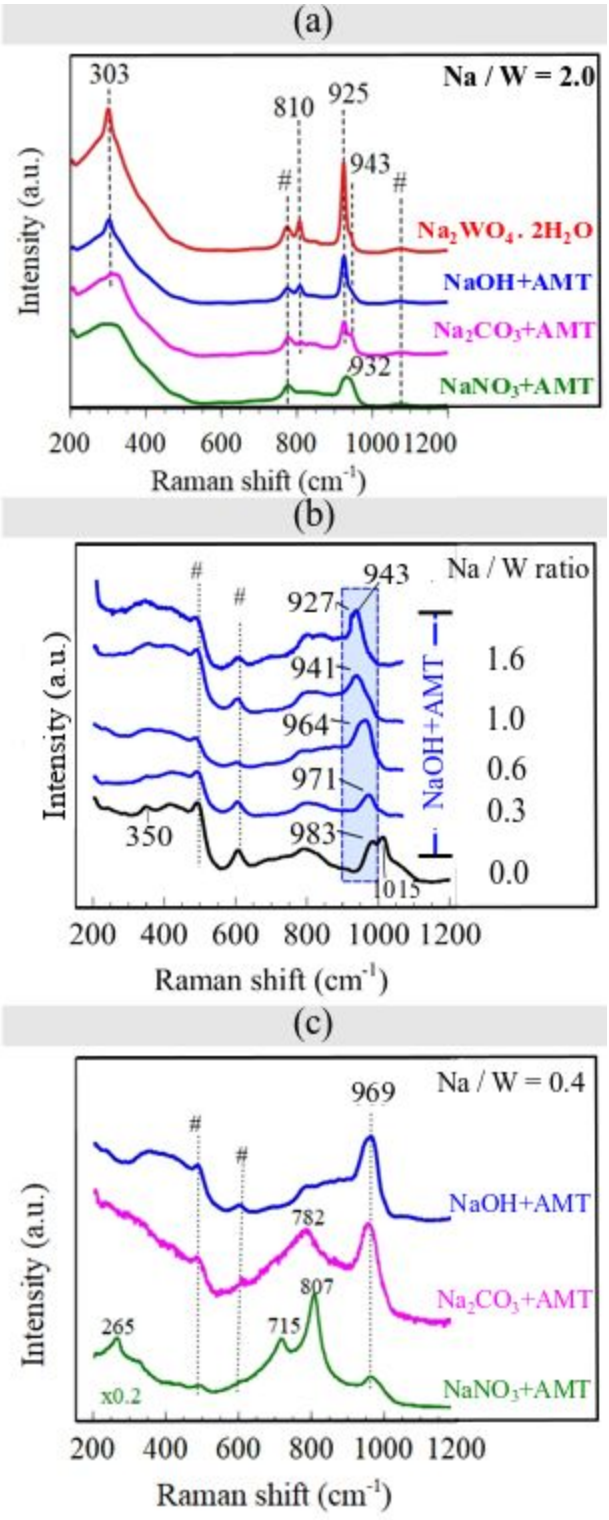

**Figure 2**. *In situ* Raman of (a) stoichiometric Na/W=2 catalysts obtained using different precursors, (b) non-stoichiometric catalysts prepared using different Na/W molar ratios, while keeping precursors (AMT+NaOH) constant. The W=O bond vibration is seen to redshift as Na/W molar ratio increases from 0.0 to 1.6 (c) non-stoichiometric Na/W= 0.4 catalysts prepared using different precursors. All spectra were collected at 400°C under dehydrated conditions. '#' indicates Raman bands originating from the $SiO_2$ support.

### b. *In situ* UV-Vis Diffuse Reflectance spectroscopy of model supported Na-$WO_x$/$SiO_2$ catalysts

The *in situ* UV-VisDR spectra for the supported 5%$Na_2WO_4$/$SiO_2$ catalysts prepared using different precursors are shown in **Figure 3** and their corresponding edge energy ($E_g$) values and ligand-to-metal-charge-transfer (LMCT) band positions are presented in **Table S1** while the corresponding Raman spectra of these catalysts are shown in **Figure 2a**. The catalysts prepared with the $Na_2WO_4 \cdot 2H_2O$ and NaOH+AMT precursors exhibit a strong LMCT band at ~214 nm and a weaker band at ~257 nm. The strong band at ~214 nm corresponds to the crystalline $Na_2WO_4$ phase.[26] The band at ~257 nm band is not present in the UV-Vis DRS spectrum of crystalline $Na_2WO_4$ and arises from the dispersed Na-$WO_4$ surface sites (*vide infra*). The shoulder at ~257 nm for the catalyst synthesized from the NaOH+AMT precursors indicates a slightly higher population of the dispersed Na-$WO_4$ surface phase than the crystalline $Na_2WO_4$ phase in comparison to the catalyst prepared using the $Na_2WO_4 \cdot 2H_2O$ precursor. For the catalysts prepared from the $Na_2CO_3$+AMT and $NaNO_3$+AMT precursors, a broad and strong UV-Vis band is present

at ~237-240 nm suggesting comparable signals from crystalline or disordered $Na_2WO_4$ and dispersed Na-$WO_4$ surface sites. The absence of UV-Vis absorption in the 400-700 nm indicates that the supported tungsten oxide phases are in their fully oxidized state ($W^{6+}$).[27] The corresponding UV-Vis $E_g$ values for these catalysts were found to be in the narrow range of 4.6-4.8 eV, which is slightly lower than that of the bulk $Na_2WO_4$ crystalline material (Eg ~ 5.3 eV), and reflect the presence of *isolated* tetrahedral $WO_4$ sites (both for crystalline/disordered $Na_2WO_4$ and dispersed Na-$WO_4$ sites).[26]

The *in situ* UV-Vis DRS spectra of the non-stoichiometric catalysts are presented in **Figure 3b** and their corresponding LMCT bands and $E_g$ values summarized in **Table S2**. The UV-Vis spectra are dominated by a broad LMCT band that shifts from 247 to 232 nm with increasing Na/W. Moreover, a continuous increase in $E_g$ value from 3.9 to 4.5 eV was also observed with increasing Na/W ratio. These trends reflect the increase in symmetry of the surface $WO_4$ sites with increasing Na/W ratio since the corresponding Raman spectra do not indicate the presence of crystalline $Na_2WO_4$ NPs or bridging W-O-W bonds from oligomeric surface $WO_x$ sites in the 200-300 $cm^{-1}$ range. Increasing the surface $WO_x$ content to 8% and decreasing the surface Na content to 0.4% results in a Na/W ratio of 0.4 (dashed plot) and yields an $E_g$ value of 4.1 eV, which is similar to previous $E_g$ value for the catalyst with Na/W ratio of 0.32. Similar to the stoichiometric catalysts (Na/W=2), the UV-Vis DRS spectra of the non-stochiometric catalysts (Na/W<2) do not contain absorption bands in the 400-700 nm range, indicating that presence of fully oxidized $W^{6+}$ sites.

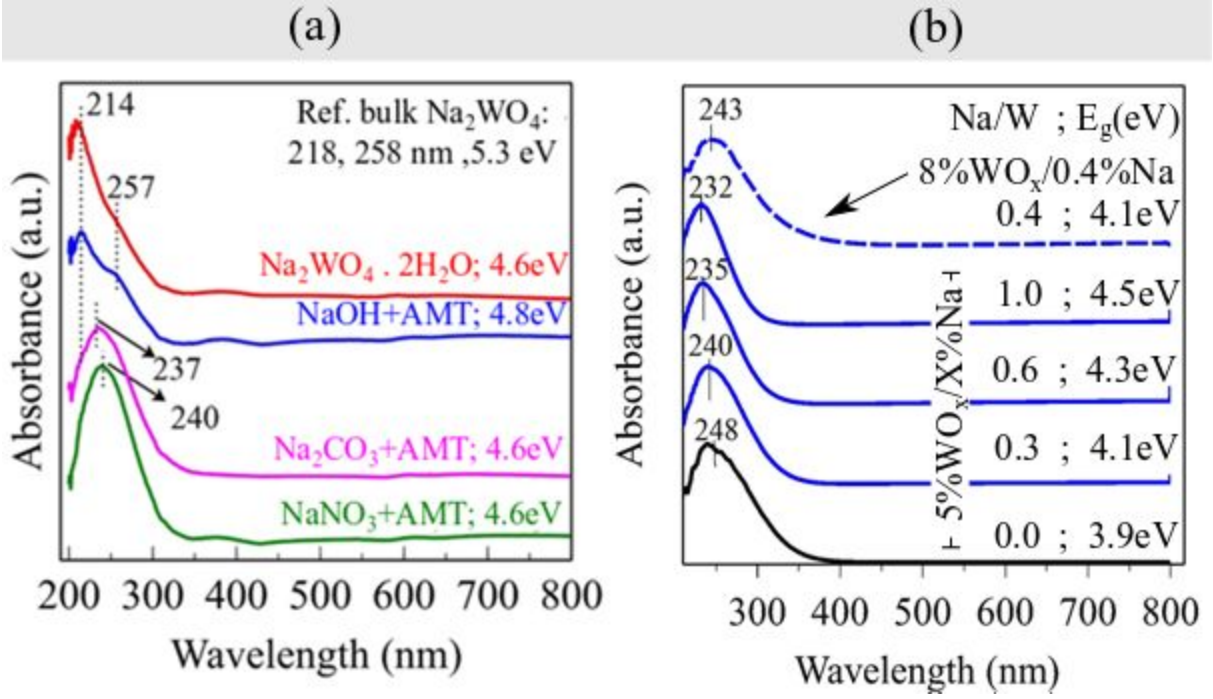


**Figure 3.** UV-DRS plots for (a) catalysts prepared using different Na and W precursors, each nominally corresponding to 5%$Na_2WO_4/SiO_2$ composition and (b) model catalysts prepared with varying Na/W molar ratio, using AMT+NaOH precursors. The dashed plot, labeled 8%$WO_x$/0.4%Na/$SiO_2$ (Na/W=0.4) is significant since such high W loading in a fully dispersed phase has not been reported before. The solid blue plots in (b) use 5%$WO_x$ loadings with corresponding Na loadings to tune Na/W.

### c. Surface acidity and basicity of model supported Na-$WO_4$ catalysts

**Surface acidity.** *In situ* $NH_3$-TPD-DRIFTS was used to study the surface acidity of dehydrated catalyst samples. The $NH_3$-TPD-DRIFT spectra for 5% $WO_x/SiO_2$-the only acidic sample as shown in **Figure S3**- are shown in **Figure 4a**, from 120 to 400°C. After $NH_3$ adsorption at 120°C, the DRIFT spectrum of the supported $WO_x/SiO_2$ catalyst with Na/W = 0 exhibited peaks corresponding to $NH_3$ adsorbed on Lewis acids sites with bands at 1334 and 1615 $cm^{-1}$ and on Brønsted acid sites as surface $NH_4^+$ ion with a band at 1437 $cm^{-1}$.[35,36] As the temperature was ramped from 120 to 400°C**,** the surface $NH_4^+$- species on Brønsted acid sites were not present beyond ~220°C while the surface $NH_3$ species on Lewis acid sites were present even at 400°C, reflecting the stronger acid strength of the surface Lewis acid sites. On the other hand, both of the Na-containing samples, i.e. the non-stoichiometric 8%$WO_x$/0.4%Na/$SiO_2$ with Na/W=0.4 and the stoichiometric 5% $Na_2WO_4/SiO_2$ with Na/W=2 exhibited no peaks due to $NH_3$ adsorbing on Lewis

or Brønsted acid sites **(Figure S3a)**. This indicated that the presence of the small Na concentrations readily removes all surface acidity in Na-$WO_x$-based catalysts.

**Surface basicity.** The DRIFT spectra obtained during $CO_2$-TPD-DRIFTS from 120 to 400°C are shown in **Figure 4b-c.** Adsorption of $CO_2$ was negligible on the supported $WO_x/SiO_2$ catalyst with Na/W=0 because of the acidic nature of the surface $WO_x$ sites (**Figure S3b**). However, $CO_2$ readily adsorbed on the Na-containing catalysts due to the interaction between acidic $CO_2$ and the basic $Na^+$ cations. For the catalyst with Na/W molar ratio of 0.4 (**Figure 4b**), $CO_2$ adsorption resulted in monodentate bicarbonate structure due to the coordination to the isolated surface $Na^+$ sites, as evidenced by the characteristic 1280 and 3730 $cm^{-1}$ bands due to the O-H bending and stretching, respectively and ~1580 $cm^{-1}$ band due to the asymmetric –COO stretching of bicarbonate (-C=O(-OH)).[35,37–40] The negative DRIFTS band at 3746 $cm^{-1}$ corresponds to the consumption of Si-OH hydroxyls on the $SiO_2$ support upon surface bicarbonate formation. Upon temperature ramp, some surface bicarbonates were still present at 400°C reflecting the strength of these isolated basic surface sites. Lastly, for the stoichiometric catalyst Na/W molar ratio of 2 (**Figure 4c**), $CO_2$ adsorbed on the surface as bidentate carbonate due to the higher surface density of $Na^+$ cations allowing for bi-ligation of the $CO_2$ molecules. IR bands at 1364 and 1610 $cm^{-1}$ bands correspond to the symmetric and asymmetric stretches of –COO from the surface $CO_3$ species.[35,37–40] TPD results reveal higher basic strength of the surface $Na^+$ sites as evidenced by the presence of strong IR peaks from surface carbonates even at ~400°C. In addition, as the temperature was increased, IR peaks at 1570 and 1280 $cm^{-1}$ increased reflecting the formation of surface bicarbonates at higher temperatures.[35,37–40] Note that as seen in **Figure S3b**, bulk $Na_2WO_4$ also exhibits the formation of bidentate carbonate species upon $CO_2$ formation, suggesting that Na density on bulk $Na_2WO_4$ and 5%$Na_2WO_4/SiO_2$ is similar.

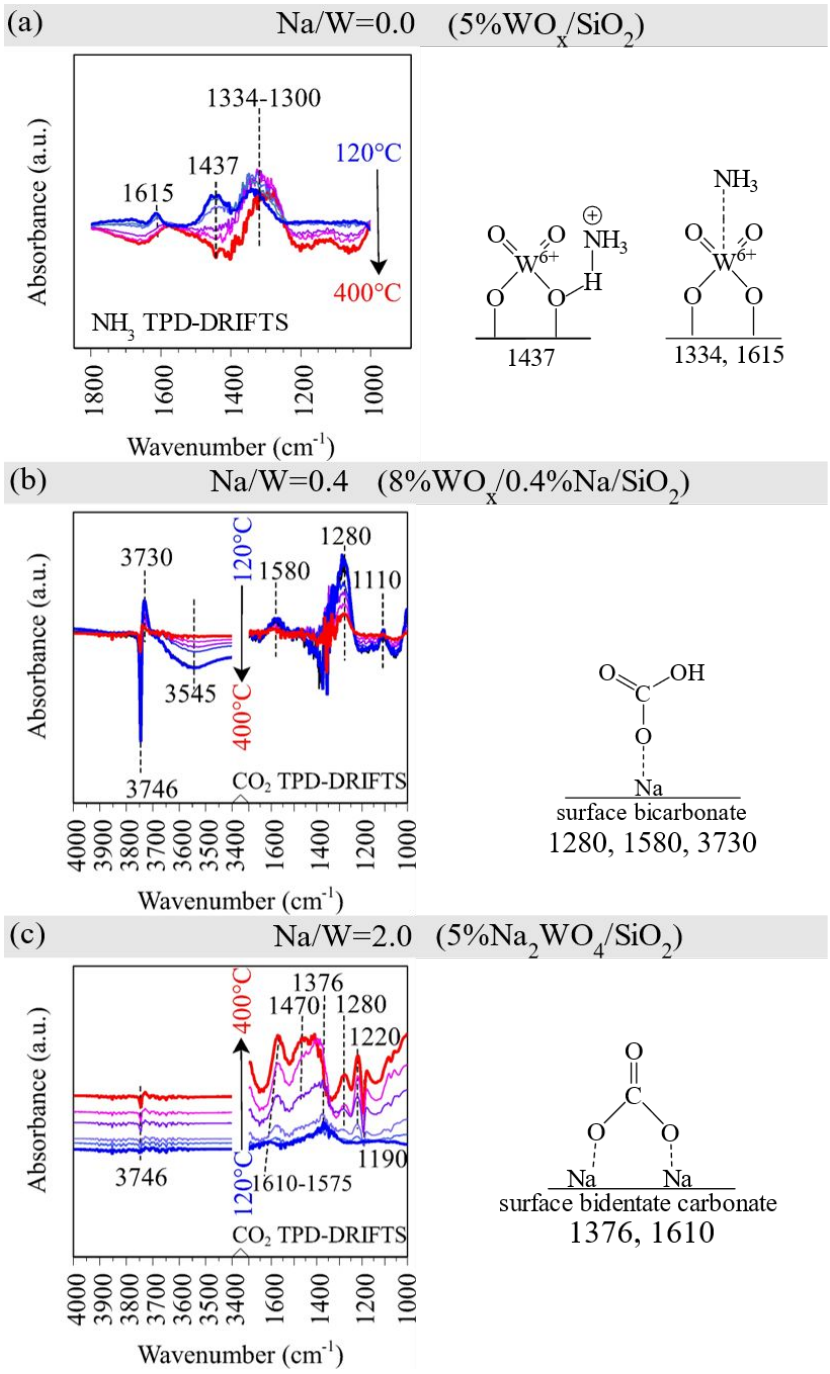


380

381

382 **Figure 4.** (a) *In situ* $NH_3$-TPD-DRIFTS of 5% $WO_x/SiO_2$ catalyst (Na/W=0), prepared using AMT
383 precursor. *In situ* $CO_2$-TPD-DRIFTS of stoichiometric (b) non-stoichiometric 8%
384 $WO_x$/0.4%Na/$SiO_2$ catalyst corresponding to Na/W= 0.4, prepared using AMT and NaOH
385 precursors, (c) stoichiometric 5% $Na_2WO_4/SiO_2$ catalyst with Na/W=2, prepared using
386 $Na_2WO_4 \cdot 2H_2O$ precursor. The corresponding molecular structures of the adsorbed species are
387 shown next to DRIFTS plot in each case.

### d. Temperature-progammed chemical probing studies.

**$H_2$-TPR.** The $H_2$-TPR $T_p$ values of the dispersed supported catalysts are sensitive to the Na/W ratio and continuously decreases from ~890-690°C with increasing Na/W ratio. For the highest Na loading of Na/W=1.6 shown in **Figure 5a**, an additional reduction peak at ~760°C was observed, which corresponds to the reduction of crystalline $Na_2WO_4$ *(vide infra)*. The $H_2$-TPR spectra of the stoichiometric (Na/W=2) 5% $Na_2WO_4/SiO_2$ catalysts prepared by utilizing different precursors for Na and W oxides are presented in **Figure 5b**. The catalyst prepared with $Na_2WO_4{\cdot}2H_2O$ precursor which contains the highest amount of crystalline $Na_2WO_4$ phase as shown by the Raman spectra in **Figure 2** and exhibits a strong reduction peak ~740°C and a broad reduction peak between 550-700°C ($T_p$~640°C) originating from crystalline $Na_2WO_4$ and dispersed Na-$WO_4$ sites, respectively. The deconvolution of the two reduction regimes was undertaken and a ratio of the contribution of dispersed Na-$WO_4$ sites to the crystalline $Na_2WO_4$ phase towards the total reduction profile is given in **Table S3**. These $H_2$-TPR features are also present for other catalysts (5%$Na_2WO_4/SiO_2$ prepared from AMT+NaOH and AMT+$Na_2CO_3$) with slight shifts in the $T_p$ values. Namely, (*i*) the $T_p$ value for the $Na_2WO_4$ NPs shifts from ~740 to ~690°C as the particle size decreases because of the easier reduction of smaller particles and (*ii*) the $T_p$ values for the dispersed Na-$WO_4$ sites are strongly dependent on the quantity of interacting surface Na cations and shift from ~890 to 640°C. The $H_2$-TPR spectrum of the catalyst prepared from the AMT+$NaNO_3$ precursors is the most unusual since this sample doesn't exhibit the Raman features of crystalline $Na_2WO_4$ NPs (see **Figure 2a**) and contains two broad reduction bands centered ~640 and ~820°C from surface Na-$WO_4$ species containing variable local Na concentrations, respectively. The lower $T_p$ values for the dispersed phase Na-$WO_4$ sites with the Na/W concentration much lower than 2 demonstrates that the surface non-stoichiometric Na-$WO_4$ sites can reduce with $H_2$ more readily than the crystalline $Na_2WO_4$ phase, which contains Na/W stoichiometry of 2.

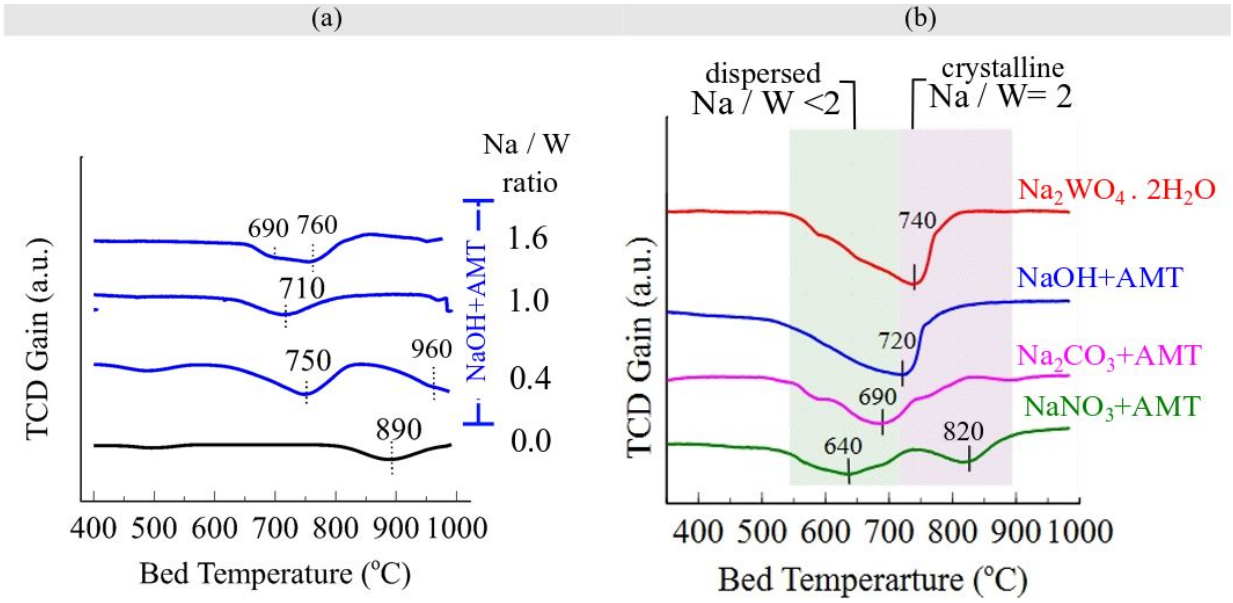


412

413 **Figure 5.** $H_2$ temperature-programmed reduction ($H_2$-TPR) for (a) non-stoichiometric, dispersed
414 phase catalysts with Na/W=0-1.6, (b) 5%$Na_2WO_4/SiO_2$ (Na/W=2) prepared with various
415 precursors.

416 **($CH_4$+$O_2$)-TPSR.** The ($CH_4$+$O_2$)-TPSR spectra for the non-stoichiometric catalyst with Na/W
417 molar ratio of 0.4 and the stoichiometric catalyst with Na/W ratio of 2 are shown in **Figure 6**. The
418 8% $WO_x$/0.4% $Na/SiO_2$ (Na/W=0.4) catalyst exhibits light-off temperature for selective product
419 $C_2H_6$ at ~650-670°C, while no $C_2H_4$ evolved over this catalyst. Unselective product, i.e CO
420 exhibits a light-off temperature of ~670°C, while appreciable amounts of $CO_2$ were not detected
421 from the catalyst. On the other hand, the light off temperatures for selective products on the
422 Na/W=2 catalyst were 570-590°C for both $C_2H_6$ and $C_2H_4$, although a strong evolution of $C_2H_4$
423 was observed above 800°C. In terms of unselective products, considerable amounts of CO and
424 $CO_2$ co-evolved with the selective $C_2$ prodcuts at 570-590°C on this catalyst.

425 The ($CH_4$+$O_2$)-TPSR results herein reveal that:

426 a) $CH_4$ conversion starts at ~570-590°C on Na/W=2, and at 670-690°C on Na/W=0.4
427 catalyst, which suggests that higher Na/W creates more reducible sites (as shown in
428 **Figure 5**), that are more active towards OCM. (Reducibility ↑, activity ↑)
429 b) The $C_2$ ($C_2H_6$+$C_2H_4$) yield is 3.3%, and $CO_x$ (CO + $CO_2$) yield is 2.4% for the Na/W=2
430 catalyst; leading to a selectivity of ~ 58% (selective yield/total yield = ~0.58). On the

other hand, for Na/W=0.4 catalyst, the $C_2$ yield is 1%, while $CO_x$ yield is 0.4%, i.e selectivity of ~71%.

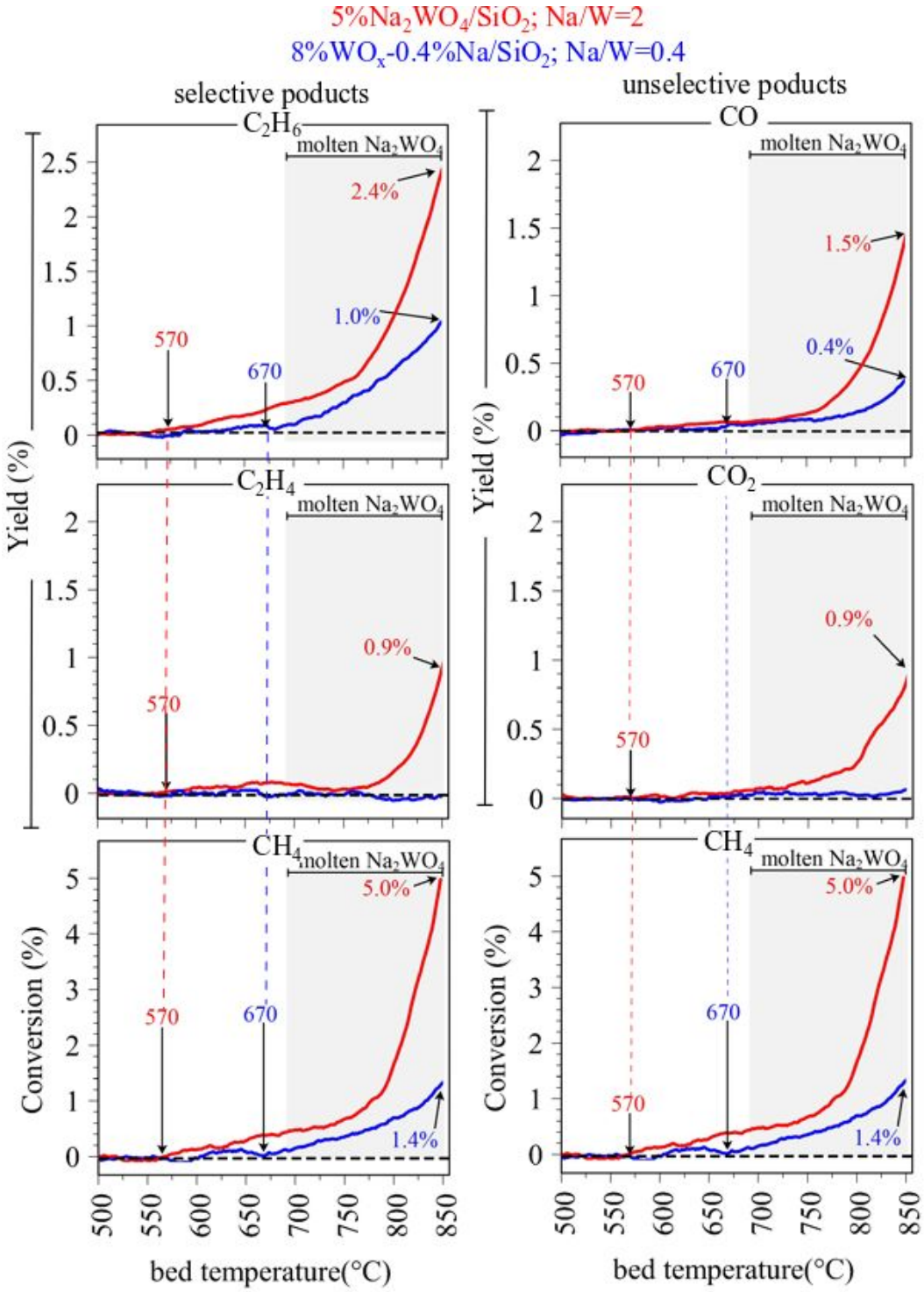

**Figure 6.** $CH_4$+$O_2$ temperature-programmed surface reaction (TPSR) for 8%$WO_x$/0.4%Na/$SiO_2$ (Na/W=0.4) shown in blue, and 5%$Na_2WO_4$/$SiO_2$ (Na/W=2) prepared from $Na_2WO_4.2H_2O$ precursor, shown in red. A heating rate of 10°C/min was used for this TPSR study.

## 4. Discussion

### a. Molecular and electronic structure of model $SiO_2$-supported tungsten oxide catalysts.

Molecular level resolved model OCM catalysts with distinct phases and molecular structures were synthesized and investigated systematically to study their molecular structure and properties. Experimental results in **Figures 2a**, **Figure S2** and **Figure 3a** show that 5% $Na_2WO_4$/$SiO_2$ OCM catalysts contain (a) a fully dispersed Na-$WO_4$ phase consisting of isolated $WO_4$ units with Na/W molar ratio less than 2, (b) a crystalline $Na_2WO_4$ phase with Na/W ratio of 2 and (c) $SiO_2$ support in the β-cristobalite phase. Interestingly, by using different Na and W oxide precursors for preparing the catalysts with the same nominal loading of ~5% $Na_2WO_4$/$SiO_2$, it was shown that the ratio between the fully dispersed Na-$WO_x$ (Raman band at ~943 $cm^{-1}$) and the crystalline $Na_2WO_4$ (Raman band at 925 $cm^{-1}$) phases could be controlled and catalysts prepared using individual Na and W precursors exhibit higher amounts of the dispersed Na-$WO_4$ surface sites.

For the Na/W<2 catalysts which contain only dispersed phase Na-$WO_4$ surface sites, the $SiO_2$ support was present in its amorphous phase instead of the crystalline β-cristobalite phase. Their molecular structure, shown in **Figure 2b**, is highly a distorted pseudo-tetrahedral $WO_4$ coordinated to Na cations that cause elongation of the W=O bond, suggested by W=O Raman band red-shifting with an increase in the Na/W ratio. This trend matches previous reports that also showed that when an alkali metal, such as K, is doped into supported $WO_x$ catalysts, the W=O vibration of the surface $WO_x$ sites shifts to lower values by 30-80 $cm^{-1}$ suggesting the strong interactions between the alkali dopant and the oxygen bound to the $WO_x$ sites.[28]. As the Na/W=2 catalysts, the Na/W <2 catalysts also exhibit a strong precursor-dependent phase generation behavior where the formation of dispersed Na-$WO_4$ surface sites is generally greater for preparations with low Na/W ratio (lower than 1.6) and the use of AMT+NaOH as the precursors. On the other hand, as seen in **Figure 2c,** crystalline phases formed when Na precursors with lower pH were used ($NaNO_3$ or $Na_2CO_3$). Finally, electronic structure information in **Figure 3b** corroborates that as the Na/W molar ratio increases, the distortion in tetrahedral geometry of the $WO_4$ units decreases, evidenced by an increase in the $E_g$ values. When the Na/W is high enough that locally it is ~2, crystalline $Na_2WO_4$

nanoparticles form and the $E_g$ increase approaches that of the bulk, unsupported crystalline $Na_2WO_4$ at 5.3eV.

In summary, the molecular structures of the $SiO_2$-supported tungsten oxide phases are strongly dependent on the synthesis method (specific precursor and Na/W ratio), which allows for controlling the distribution of various possible phases on the $SiO_2$ support. The characterization results herein clearly reveal that the Na-$WO_x/SiO_2$ catalyst can contain four distinct structural regimes. Namely, crystalline $Na_2WO_4$ with Na/W=2, crystalline $WO_3$ with Na/W=0, dispersed Na-$WO_4$ with Na/W <2, and dispersed $WO_4$ with Na/W=0. Except for the crystalline $WO_3$ phase comprised of an extensive oligomeric $W^{+6}$ sites, the three other tungsten oxide structures consist of isolated sites $W^{+6}$ centers.

**b. Nature of surface sites in model $SiO_2$-supported tungsten oxide catalysts.**

The molecular structures present in the $SiO_2$-supported tungsten oxide catalysts possess different surface acidity-basicity characteristics. The dispersed $WO_4$ surface sites and crystalline $WO_3$ nanoparticles in a catalyst with Na/W=0 exhibit surface Lewis and Brønsted acidity (see **Figure 4**). In the presence of surface Na, the acidic surface $WO_4$ sites are transformed to basic surface sites as the Na cations coordinate to $WO_x$ centers forming surface Na-$WO_4$. The degree of basicity of Na -cordinated surface $WO_4$ sites strongly depends on the Na/W ratio. At Na/W=0.4, surface mono-dentate bicarbonate species formed. On the other hand, at Na/W = 2, both in bulk $Na_2WO_4$ and in 5%$Na_2WO_4/SiO_2$, surface bidentate carbonate formed, suggesting similar surface Na density in both cases.

The redox properties of the molecular structures present in the $SiO_2$-supported tungsten oxide catalysts were probed with $H_2$-TPR. The Na-free $SiO_2$-supported $WO_4$ sites were quite stable towards the reduction and exhibited a $T_p$ value of ~890°C. The addition of Na, however, dramatically enhanced the reduction of the surface $WO_4$ sites, indicated by lowering of $T_p$ value from ~890°C (Na/W=0) to ~710°C (Na/W=1). The reduction of the $SiO_2$-supported crystalline $Na_2WO_4$ NPs varied over a smaller range from $T_p$ values of 740 to 690°C with decreasing the size of the $Na_2WO_4$ NPs. In the presence of significant concentrations of Na, thus, the ease of reduction of the surface Na-$WO_4$ NPs by $H_2$ becomes more facile[41–47]. The $H_2$-TPR reduction profiles of supported $Na_2WO_4/SiO_2$ catalysts have previously been investigated[45–47] and reported a major reduction peak at 720-750°C that was assigned to the reduction of the crystalline $Na_2WO_4$

phase.[45,47] This assignment is in agreement with the reduction peak in the 690-740°C range, for our 5%$Na_2W_4/SiO_2$ catalysts, associated with the reduction of crystalline $Na_2WO_4$ NPs. In addition to the significant reduction in the 720-750°C range, the $H_2$-TPR profiles in the literature also exhibited a weak, broad reduction peak in the lower temperature range of 625-675°C, but the authors could not explain the origin of this peak.[28,45,47] Work herein reveals, *for the first time*, that the lower $H_2$ reduction peak is due to the presence of dispersed phase Na-$WO_4$ surface sites in these catalysts that were also present in the catalysts previously reported, but not identified.

### c. Catalytic properties of surface sites in model $SiO_2$-supported tungsten oxide catalysts for OCM

. Catalytic performance of $SiO_2$ supported Na-$WO_x$ catalysts are investigated by $CH_4$+$O_2$ TPSR experimnets. These results (in **Figure 6** along with results presented in **Figure 2-5**) suggest that the 5%$Na_2WO_4/SiO_2$ catalyst with strongly basic sites present as a mixture of crystalline and dispersed phases, with Na/W=2 and Na/W<2, respectively, led to co-evolution deep-oxidation products under OCM reaction environment. However, the 8%$WO_x$/0.4%$Na/SiO_2$ catalyst, which only contains mildly basic, dispersed phase Na-$WO_4$ sites with Na/W= 0.4, suppresses the formation of deep-oxidation products, albeit their lower activity. The distinct chemical properties of stoichiometric Na/W=2 versus the non-stoichiometric Na/W=0.4 sites in $WO_x$-based catalysts towards methane activation during OCM introduce an often-overlooked parameter to tune the selectivity of the active centers by varying the Na/W ratio in these catalysts.OCM selective catalytic sites originating in the dispersed phase instead of the crystalline phase of the catalyst were acknowledged only indirectly in a recent study which concluded that reducing the overall catalyst loading reduced the size of the $Na_2WO_4$ crystallites, leading to an increase in the catalytic activity of the catalyst.[48]

Previously, a report[45] investigating the effect of using different precursors for Na and W observed that a catalyst made by impregnating $Na_2WO_4{\cdot}2H_2O$ precursor into synthetic α-cristobalite yielded a poorer catalyst than one prepared by impregnating the precursor into amorphous $SiO_2$, which then transformed into cristobalite *in situ* during calcination. The $H_2$-TPR results of the same study, for $Na_2WO_4/SiO_2$ catalyst prepared using amorphous $SiO_2$ support, reported a reduction peak at ~625°C (on the shoulder of 750°C reduction peak from crystalline $Na_2WO_4$ phase) corroborating reduction behavior observed in this work for surface Na-$WO_4$ sites with Na/W<<2. It can be

suggested that as amorphous $SiO_2$ transforms into the cristobalite phase during calcination, facile $Na^+$ ions migrate into the $SiO_2$ bulk leading to a decrease in the surface Na concentration, effectively generating dispersed phase Na-$WO_4$ surface sites with Na/W<2, which are significantly more $C_2$ selective, but less active for OCM.

Other authors investigated the interactions of Na-$WO_x$ oxides in the catalyst and concluded that the $WO_4$ tetrahedron on the 5%$Na_2WO_4/SiO_2$ catalyst was distorted by the interaction of crystalline $Na_2WO_4$ with the $SiO_2$ support.[10] This is contrary to the results presented here since crystalline $Na_2WO_4$ does not interact with the $SiO_2$ and the surface sites are responsible for the appearance of the Raman band originating in the dispersed phase Na-$WO_4$ surface sites. Lastly, it can be noted that a handful of previous reports hypothesized about the pseudo-tetrahedron $WO_4$ as being the active site for OCM.[10,19,50,51] However, none of these reports confirmed the presence of dispersed phase Na-$WO_4$ sites or the effect of Na-coordination on $WO_4$ structure. Present work shows that the presence of various catalyst phases (crystalline vs dispersed vs nanoparticles) is possible. Furthermore, the association of the activity during OCM with the $WO_4$ units in the crystalline $Na_2WO_4$ phase is inaccurate since crystalline $Na_2WO_4$ melts at ~700°C and is not present under OCM conditions.

## Conclusions.

Application of modern *in situ* physical (Raman, IR, UV–vis) and chemical probe (TPSR, TPR) spectroscopic techniques has provided new insights into supported Na-$WO_x/SiO_2$ catalysts during OCM. The traditionally prepared catalysts corresponding to 5%$Na_2WO_4$ nominal loading with Na/W molar ratio of 2, especially from $Na_2WO_4{\cdot}2H_2O$ precursor, resulted in catalysts with $SiO_2$ in the cristobalite phase co-populated with crystalline $Na_2WO_4$ (Na/W=2) and dispersed Na-$WO_4$ (Na/W<2) phases. On the contrary, catalysts prepared via modified impregnation method using individual precursors NaOH + AMT in carefully controlled proportions to maintain Na/W molar ratio well below 2, yielding catalysts with $SiO_2$ in the amorphous phase, populated only with dispersed phase Na-$WO_4$ surface sites with Na/W<2. The dispersed phase Na-$WO_4$ surface sites with Na/W<2 were found to be more geometrically distorted, less basic in nature, and more reducible than crystalline $Na_2WO_4$ (Na/W=2). Moreover, $CH_4$+$O_2$ TPSR results provide direct experimental evidence that the catalyst with only dispersed phase Na-$WO_4$ sites with Na/W<2 was less active for the formation of $CO_x$ products (hence, more selective) and initiates $C_2H_6$ formation

at higher temperature (hence, less active) than the traditional, $Na_2WO_4/SiO_2$ (Na/W=2) catalyst that contains both dispersed and crystalline phases. For the first time, the present investigation establishes the identity and crucial role of the dispersed phase, Na-coordinated, pseudo-tetrahedral $WO_4$ sites on the $SiO_2$ support surface for methane activation during OCM. Moreover, the long speculated role of the crystalline cristobalite phase of $SiO_2$ towards OCM has been experimentally disproven, since catalysts with Na/W<2 retain $SiO_2$ in the amorphous phase due to low concentrations of Na available, yet produce a better final catalyst than cristobalite supported counter part.

**Conflicts of interest.**

There are no conflicts of interest to declare

**Acknowledgments.**

This work was supported by NSF CBET award # 1706581. DK and SS performed all experimental work. DK, SS, JB, and IEW designed the experimental strategy and wrote the manuscript. The authors also gratefully acknowledge insightful input from Dr. Michael E. Ford of the *Operando* Molecular Spectroscopy & Catalysis Research Laboratory at Lehigh University.

585

586 **References.**

587 (1) Wang, B.; Albarracín-Suazo, S.; Pagán-Torres, Y.; Nikolla, E. Advances in Methane
588 Conversion Processes. *Catal. Today* **2017**, *285*, 147–158.

589 (2) Keller, G. E.; Bhasin, M. M. Synthesis of Ethylene via Oxidative Coupling of Methane: I.
590 Determination of Active Catalysts. *J. Catal.* **1982**, *73* (1), 9–19.

591 (3) Nguyen, T. N.; Nhat, T. T. P.; Takimoto, K.; Thakur, A.; Nishimura, S.; Ohyama, J.;
592 Miyazato, I.; Takahashi, L.; Fujima, J.; Takahashi, K.; et al. High-Throughput
593 Experimentation and Catalyst Informatics for Oxidative Coupling of Methane. *ACS Catal.*
594 **2020**, *10* (2), 921–932.

595 (4) Zavyalova, U.; Holena, M.; Schlögl, R.; Baerns, M. Statistical Analysis of Past Catalytic
596 Data on Oxidative Methane Coupling for New Insights into the Composition of High-
597 Performance Catalysts. *ChemCatChem* **2011**, *3* (12), 1935–1947.

598 (5) Farrell, B. L.; Igenegbai, V. O.; Linic, S. A Viewpoint on Direct Methane Conversion to
599 Ethane and Ethylene Using Oxidative Coupling on Solid Catalysts. *ACS Catal.* **2016**, *6*
600 (7), 4340–4346.

601 (6) Schwach, P.; Pan, X.; Bao, X. Direct Conversion of Methane to Value-Added Chemicals
602 over Heterogeneous Catalysts: Challenges and Prospects. *Chem. Rev.* **2017**, *117* (13),
603 8497–8520.

604 (7) Arndt, S.; Otremba, T.; Simon, U.; Yildiz, M.; Schubert, H.; Schomäcker, R. Mn–
605 Na2WO4/SiO2 as Catalyst for the Oxidative Coupling of Methane. What Is Really
606 Known? *Appl. Catal. A Gen.* **2012**, *425–426*, 53–61.

607 (8) Kiani, D.; Sourav, S.; Baltrusaitis, J.; Wachs, I. E. The Oxidative Coupling of Methane
608 (OCM) by SiO2-Supported Tungsten Oxide Catalysts Promoted with Mn and Na. *ACS*
609 *Catal.* **2019**, *9* (7), 5912–5928.

610 (9) Ji, S.; Xiao, T.; Li, S. S.-B. Ben; Xu, C.; Hou, R.; Coleman, K. S.; Green, M. L. .; Wu, J.;
611 Li, S. S.-B. Ben; Jiang, Z. C.; et al. Oxidative Coupling of Methane over Oxide-Supported
612 Sodium-Manganese Catalysts. *Appl. Catal. A Gen.* **1995**, *68* (1), 191–196.

613 (10) Wu, J.; Li, S. The Role of Distorted WO4 in the Oxidative Coupling of Methane on
614 Supported Tungsten Oxide Catalysts. *J. Phys. Chem.* **1995**, *99* (13), 4566–4568.

615 (11) Wu, J.; Li, S.; Niu, J.; Fang, X. Mechanistic Study of Oxidative Coupling of Methane over
616 Mn2O3□Na2WO4SiO2 Catalyst. *Appl. Catal. A Gen.* **1995**, *124* (1), 9–18.

617 (12) Fang, X., Li, S., Lin, J., Chu, Y. Oxidative Coupling of Methane on W-Mn Catalysts. *J.*
618 *Mol. Catal.* **1992**, *6* (6), 427–433.

619 (13) Li, S.-B. Oxidative Coupling of Methane over W-Mn/SiO2 Catalyst. *Chinese J. Chem.*
620 **2001**, *19* (1), 16–21.

621 (14) Li, S. Reaction Chemistry of W-Mn/SiO~ 2 Catalyst for the Oxidative Coupling of
622 Methane. *J. Nat. Gas Chem.* **2003**, *12* (1), 1–9.

(15) Vamvakeros, A.; Jacques, S. D. M.; Middelkoop, V.; Di Michiel, M.; Egan, C. K.; Ismagilov, I. Z.; Vaughan, G. B. M.; Gallucci, F.; van Sint Annaland, M.; Shearing, P. R.; et al. Real Time Chemical Imaging of a Working Catalytic Membrane Reactor during Oxidative Coupling of Methane. *Chem. Commun.* **2015**, *51* (64), 12752–12755.

(16) Matras, D.; Vamvakeros, A.; Jacques, S.; Grosjean, N.; Rollins, B.; Poulston, S.; Stenning, G. B. G.; Godini, H.; Drnec, J.; Cernik, R. J.; et al. Effect of Thermal Treatment on the Stability of Na-Mn-W/SiO2 Catalyst for the Oxidative Coupling of Methane. *Faraday Discuss.* **2020**.

(17) Soultanidis, N.; Zhou, W.; Psarras, A. C.; Gonzalez, A. J.; Iliopoulou, E. F.; Kiely, C. J.; Wachs, I. E.; Wong, M. S. Relating N-Pentane Isomerization Activity to the Tungsten Surface Density of WOx/ZrO2. *J. Am. Chem. Soc.* **2010**, *132* (38), 13462–13471.

(18) Ji, S.; Xiao, T.; Li, S.; Xu, C.; Hou, R.; Coleman, K. S.; Green, M. L. . H. The Relationship between the Structure and the Performance of Na-W-Mn/SiO2 Catalysts for the Oxidative Coupling of Methane. *Appl. Catal. A Gen.* **2002**, *225* (1–2), 271–284.

(19) Ji, S.; Xiao, T.; Li, S.; Chou, L.; Zhang, B.; Xu, C.; Hou, R.; York, A. P. E. E.; Green, M. L. H. H. Surface WO4 Tetrahedron: The Essence of the Oxidative Coupling of Methane over M-W-Mn/SiO2catalysts. *J. Catal.* **2003**, *220* (1), 47–56.

(20) Wachs, I. E.; Jehng, J.-M.; Ueda, W. Determination of the Chemical Nature of Active Surface Sites Present on Bulk Mixed Metal Oxide Catalysts. *J. Phys. Chem. B* **2005**, *109* (6), 2275–2284.

(21) Phivilay, S. P.; Roberts, C. A.; Puretzky, A. A.; Domen, K.; Wachs, I. E. Fundamental Bulk/Surface Structure − Photoactivity Relationships of Supported {Rh(2−y)Cr(y)O3}/GaN Photocatalysts. *J. Phys. Chem. Lett.* **2013**, *4*, 3719–3724.

(22) Phivilay, S. P.; Puretzky, A. A.; Domen, K.; Wachs, I. E. Nature of Catalytic Active Sites Present on the Surface of Advanced Bulk Tantalum Mixed Oxide Photocatalysts. *ACS Catal.* **2013**, *3*, 2920–2929.

(23) Zhu, M.; Tian, P.; Kurtz, R.; Lunkenbein, T.; Xu, J.; Schlögl, R.; Wachs, I. E.; Han, Y.-F. Strong Metal–Support Interactions between Copper and Iron Oxide during the High-Temperature Water-Gas Shift Reaction. *Angew. Chemie Int. Ed.* **2019**, *58* (27), 9083–9087.

(24) Kim, D. S.; Ostromecki, M.; Wachs, I. E. Surface Structures of Supported Tungsten Oxide Catalysts under Dehydrated Conditions. *J. Mol. Catal. A Chem.* **1996**, *106* (1–2), 93–102.

(25) Lee, E. L.; Wachs, I. E. In Situ Spectroscopic Investigation of the Molecular and Electronic Structures of SiO2 Supported Surface Metal Oxides. *J. Phys. Chem. C* **2007**, *111* (39), 14410–14425.

(26) Ross-medgaarden, E. I.; Wachs, I. E. Structural Determination of Bulk and Surface Tungsten Oxides with UV-Vis Diffuse Reflectance Spectroscopy and Raman Spectroscopy. *J. Phys. Chem. C* **2007**, *111* (41), 15089–15099.

(27) Lwin, S.; Li, Y.; Frenkel, A. I.; Wachs, I. E. Nature of WOx Sites on SiO2 and Their Molecular Structure–Reactivity/Selectivity Relationships for Propylene Metathesis. *ACS*

*Catal.* **2016**, *6* (5), 3061–3071.

(28) Ostromecki, M. M.; Burcham, L. J.; Wachs, I. E.; Ramani, N.; Ekerdt, J. G. The Influence of Metal Oxide Additives on the Molecular Structures of Surface Tungsten Oxide Species on Alumina. II. In Situ Conditions. *J. Mol. Catal. A Chem.* **1998**, *132* (1), 59–71.

(29) Wu, J.; Li, S. The Role of Distorted W04 in the Oxidative Coupling of Methane on Tungsten Oxide Supported Catalysts. *J. Phys. Chem.* **1995**, *99*, 4566–4568.

(30) Grant, J. T.; Carrero, C. A.; Love, A. M.; Verel, R.; Hermans, I. Enhanced Two-Dimensional Dispersion of Group v Metal Oxides on Silica. *ACS Catal.* **2015**, *5* (10), 5787–5793.

(31) Tian, H.; Roberts, C. A.; Wachs, I. E. Molecular Structural Determination of Molybdena in Different Environments: Aqueous Solutions, Bulk Mixed Oxides, and Supported MoO3 Catalysts. *J. Phys. Chem. C* **2010**, *114* (33), 14110–14120.

(32) Ross-Medgaarden, E. I.; Knowles, W. V.; Kim, T.; Wong, M. S.; Zhou, W.; Kiely, C. J.; Wachs, I. E. New Insights into the Nature of the Acidic Catalytic Active Sites Present in ZrO2-Supported Tungsten Oxide Catalysts. *J. Catal.* **2008**, *256* (1), 108–125.

(33) Chan, S. S.; Wachs, I. E.; Murrell, L. L.; Wang, L.; Hall, W. K. In Situ Laser Raman Spectroscopy of Supported Metal Oxides. *J. Phys. Chem.* **1984**, *88* (24), 5831–5835.

(34) Chan, S. S.; Wachs, I. E. In Situ Laser Raman Spectroscopy of Nickel Oxide Supported on γ-Al2O3. *J. Catal.* **1987**, *103* (1), 224–227.

(35) Zhu, M.; Li, B.; Jehng, J.-M. M.; Sharma, L.; Taborda, J.; Zhang, L.; Stach, E.; Wachs, I. E.; Wu, Z.; Baltrusaitis, J. Molecular Structure and Sour Gas Surface Chemistry of Supported K2O/WO3/Al2O3catalysts. *Appl. Catal. B Environ.* **2018**, *232* (January), 146–154.

(36) Kiani, D.; Belletti, G.; Quaino, P.; Tielens, F.; Baltrusaitis, J. Structure and Vibrational Properties of Potassium-Promoted Tungsten Oxide Catalyst Monomeric Sites Supported on Alumina (K2O/WO3/Al2O3) Characterized Using Periodic Density Functional Theory. *J. Phys. Chem. C* **2018**, *122*, 24190–24201.

(37) Taifan, W. E.; Li, Y.; Baltrus, J. P.; Zhang, L.; Frenkel, A. I.; Baltrusaitis, J. Operando Structure Determination of Cu and Zn on Supported MgO / SiO 2 Catalysts during Ethanol Conversion to 1 , 3-Butadiene. *ACS Catal.* **2018**, *9*, 269–285.

(38) Turek, A. M.; Wachs, I. E.; DeCanio, E. Acidic Properties of Alumina-Supported Metal Oxide Catalysts: An Infrared Spectroscopy Study. *J. Phys. Chem.* **1992**, *96* (12), 5000–5007.

(39) Keturakis, C. J.; Ni, F.; Spicer, M.; Beaver, M. G.; Caram, H. S.; Wachs, I. E. Monitoring Solid Oxide CO2 Capture Sorbents in Action. *ChemSusChem* **2014**, *7* (12), 3459–3466.

(40) Busca, G.; Lorenzelli, V. Infrared Spectroscopic Identification of Species Arising from Reactive Adsorption of Carbon Oxides on Metal Oxide Surfaces. *Mater. Chem.* **1982**, *7* (1), 89–126.

(41) Shahri, S. M. K.; Alavi, S. M. Kinetic Studies of the Oxidative Coupling of Methane over the Mn/Na2WO4/SiO2 Catalyst. *J. Nat. Gas Chem.* **2009**, *18* (1), 25–34.

(42) Mahmoodi, S.; Ehsani, M. R.; Hamidzadeh, M. Effect of Additives on Mn/SiO2 Based Catalysts on Oxidative Coupling of Methane. *Iran. J. Chem. Chem. Eng.* **2011**, *30* (1), 29–36.

(43) Ismagilov, I. Z.; Matus, E. V.; Kuznetsov, V. V.; Kerzhentsev, M. A.; Yashnik, S. A.; Larina, T. V.; Prosvirin, I. P.; Navarro, R. M.; Fierro, J. L. G.; Gerritsen, G.; et al. Effect of Preparation Mode on the Properties of Mn-Na-W/ Sio2catalysts for Oxidative Coupling of Methane: Conventional Methods vs. POSS Nanotechnology. *Eurasian Chem. J.* **2016**, *18* (2), 93–110.

(44) Fleischer, V.; Steuer, R.; Parishan, S.; Schomäcker, R. Investigation of the Surface Reaction Network of the Oxidative Coupling of Methane over Na2WO4/Mn/SiO2 Catalyst by Temperature Programmed and Dynamic Experiments. *J. Catal.* **2016**, *341*, 91–103.

(45) Palermo, A.; Holgado Vazquez, J. P.; Lee, A. F.; Tikhov, M. S.; Lambert, R. M. Critical Influence of the Amorphous Silica-to-Cristobalite Phase Transition on the Performance of Mn/Na2WO4/SiO2 Catalysts for the Oxidative Coupling of Methane. *J. Catal.* **1998**, *177* (2), 259–266.

(46) Malekzadeh, A.; Abedini, M.; Khodadadi, A. A.; Amini, M.; Mishra, H. K.; Dalai, A. K. Critical Influence of Mn on Low-Temperature Catalytic Activity of Mn/Na2WO4/SiO2 Catalyst for Oxidative Coupling of Methane. *Catal. Letters* **2002**, *84* (1), 45–51.

(47) Tang, L.; Choi, J.; Lee, W. J.; Patel, J.; Chiang, K. Metal Effects in Mn-Na2WO4/SiO2 upon the Conversion of Methane to Higher Hydrocarbons. *Adv. Energy Res.* **2017**, *5* (1), 13–29.

(48) Hayek, N. S.; Lucas, N. S.; Warwar Damouny, C.; Gazit, O. M. Critical Surface Parameters for the Oxidative Coupling of Methane over the Mn–Na–W/$SiO_2$ Catalyst. *ACS Appl. Mater. Interfaces* **2017**, *9* (46), 40404–40411.

(49) Jiang, Z. C.; Yu, C. J.; Fang, X. P.; Li, S. Ben; Wang, H. L. Oxide/Support Interaction and Surface Reconstruction in the Sodium Tungstate(Na2WO4)/Silica System. *J. Phys. Chem.* **1993**, *97* (49), 12870–12875.

(50) Kou, Y.; Zhang, B.; Niu, J.; Li, S.; Wang, H.; Tanaka, T.; Yoshida, S. Amorphous Features of Working Catalysts: XAFS and XPS Characterization of Mn/Na2WO4/SiO2as Used for the Oxidative Coupling of Methane. *J. Catal.* **1998**, *173* (2), 399–408.

(51) Pengwei, W.; Guofeng, Z.; Wang, Y.; Yong, L.; Wang, P.; Zhao, G.; Wang, Y.; Lu, Y. MnTiO3-Driven Low-Temperature Oxidative Coupling of Methane over TiO2-Doped Mn2O3-Na2WO4/SiO2catalyst. *Sci. Adv.* **2017**, *3* (6), 1–10.

740

741

742

743 **Table of Contents Figure**

744

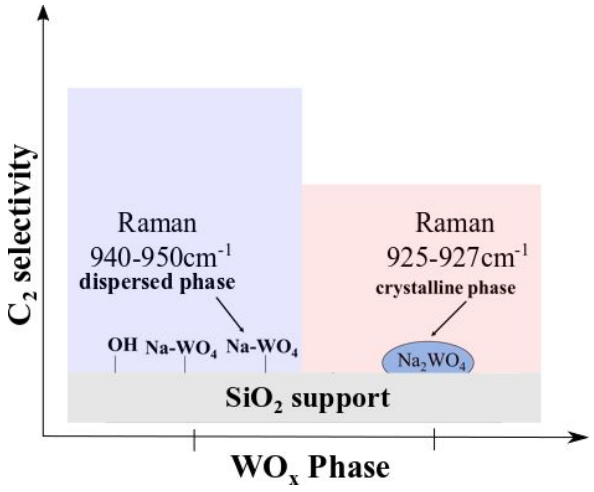


745

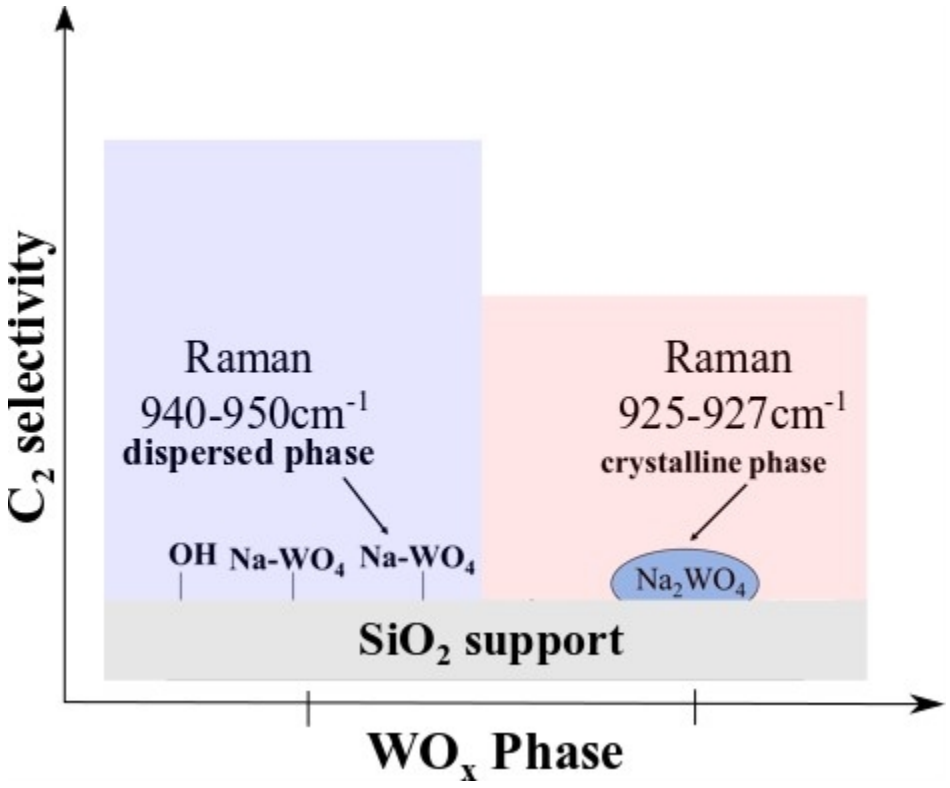


124x102mm (96 x 96 DPI)